Journal of Contaminant Hydrology 247 (2022) 103984

Contents lists available at ScienceDirect

Journal of Contaminant Hydrology

journal homepage: www.elsevier.com/locate/jconhyd

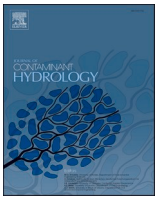

Comparison of methods to estimate air-water interfacial areas for evaluating PFAS transport in the vadose zone

Jeff A.K. Silva [a,*], Jiří Šimůnek [b], John E. McCray [c]

[a] Arclight Research & Consulting, Golden, CO, USA
[b] Department of Environmental Sciences, University of California-Riverside, USA
[c] Hydrologic Science and Engineering Program, Civil & Environmental Engineering Department, Colorado School of Mines, Golden, USA

ARTICLE INFO

Keywords:
PFAS
Air-water interfacial adsorption
Air-water interfacial area
Vadose zone transport
Soil texture and surface roughness effects
Modeling

ABSTRACT

When performing calculations or numerical simulations for the fate and transport of PFAS and other surface-active solutes in the vadose zone, accurately representing the relationship between the area of the air-water interfaces (A_{aw}) as a function of water saturation (S_w), and changes in that relationship resulting from changes in soil texture, are equally important as accurately characterizing interfacial adsorption coefficients and the concentration dependence for PFAS solutes. This is true because the magnitude of the A_{aw} directly governs the degree of air-water interfacial adsorption, which contributes to the transport retardation of these solutes within unsaturated porous media. Herein, a well-known thermodynamic-based model for predicting the A_{aw}-S_w relationship is evaluated through comparisons to literature data collected using various measurement techniques for model sands and a limited number of soils using data collected from the current published literature. This predictive model, herein termed the Leverett thermodynamic model (LTM), relies on the characterization of the soil-water retention curve (SWRC) for a given soil, using the van Genuchten (VG) equation for the pressure head-vs-S_w relationship. Therefore, methods to estimate the VG equation parameters are also compared as to the A_{aw}-S_w relationships predicted. Comparisons suggest that the LTM provides the best estimate of the actual A_{aw}-S_w relationships for water containing non-surface-active solutes. Because PFAS solutes are also surface-active, A_{aw} measurement methods utilizing surface-active tracers are considered to provide the most accurate representation of the A_{aw}-S_w relationship for these solutes. Differences between A_{aw}-S_w relationships derived from tracer methods and the LTM are described in relation to media surface roughness effects. Based on the available literature data, a practical empirical model is proposed to adjust the LTM prediction to account for the effects of surface roughness on the magnitude of the A_{aw} for surface-active solutes. Finally, example retention calculations are performed to demonstrate the sensitivity of the predicted A_{aw}-S_w relationship on the vadose zone transport of a representative PFAS, perfluorooctane sulfonate.

1. Introduction

Per- and polyfluoroalkyl substances (PFAS) are a class of emerging contaminants that have received significant attention in recent years due to human health concerns, their widespread use and distribution in the environment, and their general resistance to degradation in the environment. PFAS groundwater contamination is often associated with the leaching of these compounds from commercial products initially deposited in unlined landfills or on the ground surface (e.g., from land-applied bio-solids and past releases of aqueous film-forming foam (AFFF) products at fire training areas). In these release scenarios, PFAS must first transport through the vadose zone prior to reaching underlying aquifers. PFAS has been shown to accumulate within the shallow vadose zone, serving as a long-term source of groundwater contamination (Shin et al., 2011; Xiao et al., 2015; Weber et al., 2017; Anderson et al., 2006; Anderson et al., 2019). Therefore, it is important to understand and characterize PFAS fate and transport mechanisms within the vadose zone to better assist environmental risk assessment and future remediation decision-making.

PFAS are surface-active chemicals (i.e., surfactants). As surfactants, PFAS will accumulate at fluid interfaces during transport through the vadose zone. Of particular interest in this paper is the adsorption of PFAS

* Corresponding author.
E-mail address: jsilva@arclightrc.com (J.A.K. Silva).

https://doi.org/10.1016/j.jconhyd.2022.103984
Received 19 July 2021; Received in revised form 22 February 2022; Accepted 27 February 2022
Available online 7 March 2022

at air-water interfaces (AWI), although other important interfacial processes have been identified as additional contributors to overall PFAS retention (e.g., Guelfo and Higgins, 2013; McKenzie et al., 2016; Brusseau, 2018). PFAS adsorption at AWIs is significant under certain conditions (e.g., Brusseau, 2018; Silva et al., 2019; Guo et al., 2020; Silva et al., 2020), depending on the specific surface activity of a given PFAS and the magnitude of the area of the AWI (A_{aw}). A_{aw} is inversely related to volumetric water content (θ_w) or water saturation ($S_w = \theta_w/porosity$). Variability in A_{aw} depends on the particle size distribution in water content, which in turn depends on textural properties of the vadose zone soil. Each of these dependencies can vary spatially and temporally within the vadose-zone environment, complicating transport calculations.

Methods to characterize the A_{aw}-S_w relationship have included theoretical models (based on empirical relationships or assumptions of pore geometry [e.g., Leverett, 1941; Bradford and Leij, 1997; Gvirtzman and Roberts, 1991; Or and Tuller, 1999; Oostrom et al., 2001; Jiang et al., 2019]) and experimental measurement methods utilizing surface-active gas-phase and aqueous-phase chemical tracers (e.g., Kakare and Fort, 1996; Kim et al., 1997; Silva, 1997; Kim et al., 1999; Schaefer et al., 2000; Costanza-Robinson, 2001; Silva et al., 2002; Araujo et al., 2015; Brusseau et al., 2020). More recently, direct imaging via x-ray microtomography (XMT) methods have additionally been employed (e.g., Brusseau et al., 2007; Costanza-Robinson et al., 2008; Araujo and Brusseau, 2020). The various methods used for A_{aw} measurement methods have been shown to provide different A_{aw} values for a given S_w value, as well as different A_{aw}-S_w relationships, particularly at lower *moisture* conditions. For example, XMT methods provide linear A_{aw}-S_w relationships throughout the entire range of S_w. Gas-phase tracer methods (i.e., those in which a gaseous or vaporous tracer is introduced to a mobile air phase and where the aqueous-phase and A_{aw} are assumed static) typically provide highly non-linear A_{aw}-S_w relationships and A_{aw} values are considerably greater than those provided by other measurement methods.

With respect to aqueous tracer methods, there are two main types. The first type involves introducing the interfacial tracer with aqueous advection wherein the tracer contacts the available interfacial area under steady unsaturated flow (e.g., Brusseau et al., 2015 and references therein). For the second method, the tracer solution is introduced to an unsaturated sand column and the A_{aw} is estimated via a mass balance calculation from the equilibrium mass of tracer lost from the test column when allowed to drain to a steady-state moisture condition (Schaefer et al., 2000; Araujo et al., 2015). Schaefer et al. (2000) observed linear A_{aw}-S_w relationships while Araujo et al. (2015), using similar methods, observed a non-linear increasing trend in A_{aw} with increasing S_w. Both gaseous and aqueous tracer methods provide A_{aw} values that are greater than those derived from XMT measurements at the same S_w condition and the differences increase with decreasing S_w. The differences in A_{aw} values provided by the different measurement methods has been argued to result from each method characterizing different fractions of the total A_{aw} (e.g., A_{aw} associated with capillary-held pendular water and A_{aw} associated with thin water films adsorbed to mineral surfaces) (e.g., Costanza-Robinson, 2001; Brusseau et al., 2006).

The variability in A_{aw}-S_w relationships presented in the literature can lead to confusion over which relationships are most appropriate when performing fate and transport calculations for PFAS or other surface-active solutes. The most commonly held view based on the collective literature to date is to use A_{aw}-S_w relationships that best represent the transport conditions being investigated. For PFAS of current environmental concern, transport within the vadose zone occurs in the aqueous phase and A_{aw}-S_w relationships derived from aqueous-based methods would therefore be most representative (Silva et al., 2020; Guo et al., 2020: Brusseau et al., 2020; Brusseau et al., 2019), as these methods are considered to characterize A_{aw} accessible to surface-active solutes present in the aqueous phase. However, discrepancies between these methods remain, and too little data representative of a variety of soil types are available to make a clear judgment on the utility of the A_{aw}-S_w relationships provided. Likewise, the diversity of theoretical models available in the literature to predict the A_{aw}-S_w relationship for a given porous media adds to the complexity and uncertainty.

Herein, the efficacy of one of several theoretical models to predict A_{aw}-S_w relationships, a modification of the thermodynamic-based model first conceptualized by Leverett (1941), hereafter referred to as the Leverett Thermodynamic Model (LTM), is evaluated. Data used in this evaluation represents a variety of model porous media and natural sandy soils, with the goal of improving the accuracy of transport calculations for PFAS and other similarly surface-active solutes. This theoretical model has been used to simulate colloid and bacteria transport (Šimůnek et al., 2016) and was recently implemented in an additional modified version of the HYDRUS unsaturated flow and transport model to simulate PFAS transport in the vadose zone (Silva et al., 2020). Predicted results are compared to A_{aw}-S_w relationships derived from the literature that utilized XMT and aqueous tracer-based measurements. A_{aw}-S_w relationships predicted by the LTM method are directly dependent on the characteristics of the soil-water retention curve (SWRC) for a given porous media. Here, the well-known van Genuchten (VG) equation was selected to model SWRCs. Therefore, evaluation and discussion of the impact of key VG equation parameters on predicted A_{aw}-S_w relationships are additionally provided. Finally, an empirical relationship is proposed that can be used to scale the LTM to be more representative of A_{aw} values measured by surface-active solutes, thereby improving estimates of PFAS retention within the vadose zone due to AWI adsorption.

2. Materials and methods

2.1. AWI area calculation

The method used here to estimate A_{aw} as it changes with soil water content (θ) was proposed by Leverett (1941) and implemented by Bradford et al. (2015) as:

$$A_{aw}(\theta) = \frac{1}{\gamma_o}\int_{\theta}^{\theta_s} P_c(\theta)d\theta = \frac{\rho_w g}{\gamma_o}\int_{\theta}^{\theta_s} h(\theta)d\theta \tag{1a}$$

$$\frac{dA_{aw}(\Theta)}{d\theta} = \frac{P_c}{\gamma_o} = \frac{\rho_w g h}{\gamma_o} \tag{1b}$$

where θ_s is the saturated water content (L^3/L^3), P_c is the capillary pressure (M/LT^2), h is the pressure head (L), γ_0 is the air-water surface tension (M/T^2), ρ_w is the density of water (M/L^3), and g is the gravitational acceleration (L/T^2). The integration provides A_{aw} in units of L^2/L^3 (or L^{-1}), where the L^3 term in the numerator is the total volume of air, water, and solid phases. The magnitude of A_{aw} increases with decreasing θ and approaches the geometric surface area (GSA) of the porous media as θ approaches the residual (irreducible) water content (θ_r).

This approach relies on a specific model characterizing the change in water content in response to a change in h. Here, we selected the well-known van Genuchten (VG) model (van Genuchten, 1980):

$$\theta(h) = \begin{cases} \theta_r + \dfrac{\theta_s - \theta_r}{\left[1 + |\alpha h|^n\right]^{1-1/n}} & h \le 0 \\ \theta_s & h > 0 \end{cases} \tag{2}$$

where θ_r has units of L^3/L^3), α (1/L) is a parameter related to the inverse of the air-entry pressure head for the porous medium, and n (−) is a parameter related to the pore-size distribution. Eq. (1) describes the soil-water retention curve (SWRC) for a porous medium.

The use of Eq. (1) and similar methods to estimating A_{aw}-S_w relationships have been previously referred to as the "thermodynamic" approach (e.g., Dalla et al., 2002; Grant and Gerhard, 2007; Schroth et al., 2008;) because, as proposed by Leverett (1941), it relates changes in A_{aw} to the thermodynamic work done within a unit volume of

unsaturated porous media when changes in water contents occur due to changes in capillary pressure. The integration of Eq. (1), i.e., the area under the SWRC, yields the A_{aw}-S_w relationship. The endpoint of the A_{aw} prediction is the θ_r for a given porous medium, where it is assumed that soil moisture exists as pendular water and as a thin adsorbed layer of water coating mineral surfaces, and advective flow does not occur. This model is hereafter referred to as the Leverett thermodynamic model (LTM). The LTM is applicable strictly at the continuum (or representative elementary volume (REV)) scale, similar to the SWRC. Therefore, media characteristics not captured by the SWRC would not be represented in the A_{aw} predicted by the LTM.

2.2. X-ray microtomography dataset

The results of the LTM predictions are compared to those presented by Costanza-Robinson et al. (2008), who reported A_{aw}-S_w relationships developed from synchrotron x-ray microtomography (XMT) measurements for glass bead media and model sands. The XMT method is an imaging methodology that allows for the direct calculation of the A_{aw}-S_w relationships. The current interpretation of the XMT method results is that the A_{aw}values provided represent the combined contributions of the areas associated with capillary water (e.g., pendular rings at points of contact between mineral particles) and adsorbed water films on wetted surfaces within the pores (e.g., Brusseau et al., 2007; Costanza-Robinson et al., 2008). XMT cannot resolve interfacial area associated with microscale surface heterogeneity (e.g., surface roughness), when present, and thus provides maximal A_{aw} values that are nearly equivalent to the calculated smooth specific surface area of the porous media (Brusseau et al., 2007; Costanza-Robinson et al., 2008).

As presented by Costanza-Robinson et al. (2008), XMT provided linear A_{aw}-S_w relationship models for each media type that had the following form (after Araujo and Brusseau, 2020):

$$A_{aw} = GSA(1 - S_w) \tag{3}$$

where GSA is the geometric surface area of the medium (L^2/L^3) based on the smoothed-sphere assumption (i.e., the medium is composed of a collection of smooth spheres of an identical diameter), calculated as:

$$GSA = 6(1 - n)/d_{50} \tag{4}$$

where n is the media porosity (L^3/L^3) and d_{50} is the median particle diameter (L). Costanza-Robinson et al. (2008) actually derived the following equation: $A_{aw} = SA(0.9031 - 0.9112S_w)$. However, through our analysis, we have found Eq. (4) to be a reasonable simplification to represent the measured data presented by Costanza-Robinson et al. (2008). Hereafter, Eq. (3) will be used to represent the XMT-measured data for the soils used in this work.

2.3. Additional soil properties data

Additional soil properties data were derived from literature sources for two natural sands (Torrens et al., 1998; Costanza-Robinson, 2001; Brusseau et al., 2006; Peng and Brusseau, 2012) and used for comparison of LTM predictions. For example, measured VG parameters for two desert soils (i.e., Vinton sandy soil and Hayhook sandy loam) were obtained from the literature (Peng and Brusseau, 2012) and directly used to develop A_{aw}-S_w relationships via the LTM approach. Soil textural data (i.e., percentages of sand, silt, and clay) were also derived from the literature for the same Vinton soil (Costanza-Robinson, 2001) and Hayhook soil (Torrens et al., 1998) that were used to develop VG parameters via the well-known Rosetta Lite (v. 1.1) neural network model using the SSCBD (or H3) model described by Schaap et al. (2001), which included the bulk density (ρ_b) of the media as an additional predictive parameter. Finally, the LTM approach was applied to VG parameter data (i.e., specifically α and n values) derived from the pedotransfer function (PTF) presented by Benson et al. (2014), as described below.

2.4. Estimating VG model α and n parameters

VG model parameters α and n for each media type evaluated in this work were developed using the pedotransfer function presented by Benson et al. (2014) (hereafter referred to as the Benson PTF), which allows correction of VG parameters α and n for changes in the particle size distribution based on changes in the uniformity coefficient (C_u). For α as 1/kPa (drying curve case, from Benson et al., 2014):

$$\alpha_{1d} = 1.34 d_{60} \tag{5}$$

$$N_\alpha = 0.99 C_u^{-0.54} \tag{6}$$

where α_{1d} is the α for $C_u = 1$, N_α is α normalized by α_{1d}, and α corrected for C_u is $\alpha_{1d}N_\alpha$. d_{60} is the particle diameter (L) of which 60% of the particles in the soil sample are finer. Similarly, n (drying curve) is calculated as:

$$n_{1d} = 14 exp(-0.434 d_{60}) \tag{7}$$

$$N_n(C_u > 2.2) = -0.0033 C_u + 0.379 \tag{8}$$

where n_{1d} is the n for $C_u = 1$, N_n is n normalized by n_{1d}, and n corrected for C_u is $n_{1d}N_\alpha$. The Benson PTF utilizes regressions based on d_{60} for the media (i.e., the soil particle diameter for which 60% of the total are finer by weight). The d_{60} values for the media used here were not reported; however, the d_{50} values were. For reasonably uniform porous media, the near equivalence of d_{60} and d_{50} values can be and was assumed herein.

3. Results and discussion

3.1. Porous media properties

Porous media properties and VG parameters compiled and calculated for this evaluation are provided in Table 1. For the various glass bead media, calculated VG parameters α and n are consistent with both measured values as well as values calculated using alternative theoretical packing arrangements of spherical particles (Benson et al., 2014; Sweijen et al., 2017). Likewise, calculated α and n are consistent with reported measured values for the Accusand media (Schroth et al., 1996). According to the Benson PTF, α values follow a linearly increasing trend with increasing values of the d_{60} for these media. Calculated n values trend as a decreasing power-law function with increasing C_u. For the Vinton soil, α an n values show some variability for the different parameter estimation methods used (i.e., coefficients of variation (CV) = 25% and 15% for the estimates of α and n, respectively). The estimated values are reasonable for this type of soil.

3.2. VG parameters α and n and the effect on A_{aw} prediction

The effect of soil texture on the values of the VG equation α and n parameters used to represent the SWRC is well known. For clean sands and other coarse granular porous media, there is a strong relationship between particle/pore-size distribution and the character of the SWRC (Yang et al., 1994; Benson et al., 2014). For uniform porous media, a decrease in α relates to an increase in the air entry pressure/suction, with a slight increase in the slope of the SWRC (i.e., a decrease in the magnitude of n) between θ_s and θ_r as the particle size becomes finer. As the particle-size distribution becomes increasingly non-uniform, air entry pressures, and thus the value of α, will vary depending on the nature of the particle-size distribution and corresponding changes in particle packing arrangements. However, it is the slope of the SWRC, and thus the magnitude of n, that is most affected by the degree of particle-size non-uniformity.

When using Eq. (1) and Eq. (2) to describe the A_{aw}-S_w relationship, the impacts of α and n on the shape of the SWRC are described below. SWRCs and their corresponding A_{aw}-S_w relationships calculated for the

Table 1
Porous media properties and VG parameters collected or calculated for this evaluation.

Reference for porous media characteristics	Media	Porous media characteristics						VG equation parameters			
		d_{50} (mm)	d_{10} (mm)	C_u[a]	GSA (cm^{-1})	SSA_{BET}[b] (cm^{-1})	SRF[c]	θ_r	θ_s	α (cm^{-1})	n
	Glass Beads										
	Fine	0.099	0.090	1.1	365	780	2	0.05	0.398	0.012	13.0
	Medium	0.345	0.288	1.2	113	211	2	0.02	0.350	0.041	11.1
	Coarse	0.650	0.591	1.1	55	296	5	0.02	0.404	0.081	10.3
	Mixture	0.403	0.088	4.6	97	545	6	0.02	0.348	0.023	4.40
	Accusand Sands										
	Medium	0.375	0.313	1.2	101	1776	18	0.02	0.369	0.045	10.91
	Coarse	0.516	0.430	1.2	73	2103	29	0.02	0.372	0.061	10.26
	Granusil Sands										
	Fine	0.200	0.118	1.7	162	8473	52	0.05	0.425	0.024	8.19
	Coarse	0.513	0.302	1.7	65	5648	87	0.05	0.430	0.061	7.15
Costanza-Robinson et al. (2008)	Mixture	0.211	0.073	2.9	163	5175	32	0.05	0.427	0.022	4.85
	Vinton Sandy Soil										
	Vinton (Benson PTF)	–	–	–	–	–	–	0.05	0.419	0.019	4.83
	Vinton (measured)[d]	0.234	0.098	2.4	155	51,684	334	0.06	0.390	0.026	3.66
	Vinton (Rosetta)[e]	–	–	–	–	–	–	0.05	0.360	0.032	3.85
	Hayhook Loamy Sand										
	Hayhook (Benson PTF)	–	–	–	–	–	–	0.05	0.360	0.008	4.20
	Hayhook (measured)[d]	0.260	0.016	16	148	144,320	978	0.05	0.390	0.024	2.26
Costanza-Robinson et al. (2008); Peng and Brusseau, 2005, 2012)	Hayhook (Rosetta)[e]	–	–	–	–	–	–	0.05	0.352	0.033	1.96
Araujo and Brusseau (2020)	**1.1 mm Glass Beads**	1.1	1.1	1	32	28	0.9	0.01	0.340	0.152	8.46

Note: Porous media characteristics presented were derived from the sources cited in the table (leftmost column). VG equation parameters were calculated using the Benton PTF or as otherwise derived from sources identified in the table by footnote. [a]$C_u = d_{60}/d_{10}$ or d_{50}/d_{10} as an estimate in this case. [b]reported specific surface area from N_2/BET, where BET is the Brunauer-Emmett-Teller equation. [c]SRF is the shape/roughness factor = SSA_{BET}/GSA. [d]measured VG parameters as reported by Brusseau et al. (2006). [e]VG parameters estimated using Rosetta program (Schaap et al., 2001) and the texture-bulk density model (97% sand, 1.8%silt, 1.2% clay, bulk density = 1.63). Θ_r values derived from Benson et al. (2014), Schroth et al. (1996), Sakaki and Illangasekare (2007), Brusseau et al. (2006). VG parameters for 1.1 mm glass beads derived using Benson PTF.

glass beads and model sands used in this evaluation are presented in Fig. 1. As demonstrated for the uniform and spherical glass beads (Fig. 1a and d), a decrease in particle size, and a corresponding decrease in α, results in an increase in the air-entry pressure for the SWRC and a corresponding increase in the overall slope of the A_{aw}-S_w relationship. Mathematically, increased A_{aw} with decreasing particle size occurs due to the overall increase in the integrated area under the SWRC. Mechanistically, however, a reduction in particle size relates to an increase in the GSA, and thus an overall increase in calculated A_{aw} for $S_w < 1$. As demonstrated for the glass bead mixture, the reduction in n increases the degree of curvature of the A_{aw}-S_w relationship as S_w decreases, which is also the case for the corresponding SWRC.

The A_{aw}-S_w relationships for the Granusil sand mixture also exhibit an increasing degree of curvature, albeit less than those observed for the spherical glass beads. In this case, the A_{aw} values predicted are overall greater than those predicted for the glass bead mixture despite the fact that the C_u for the glass bead mixture is a factor of 1.6 greater than that of the Granusil mixture. The differences in these A_{aw}-S_w relationships are the result of the differences in the d_{50} reported for these sand mixtures, which impact the α and n values provided by the Benson PTF. From this analysis, it is observed that for uniform sandy porous media, the particle (pore) size – and thus the magnitude of α – plays a dominant role in the magnitude of A_{aw} values predicted by the LTM. As the particle size distribution becomes increasingly less uniform (i.e., a wider particle size distribution), the contribution of the n parameter to the predicted A_{aw} values become increasingly important.

3.3. Comparing literature-derived XMT results to LTM predictions

The results of Eq. (3), based on the XMT results presented by Costanza-Robinson et al. (2008), are represented in Fig. 1 to provide a comparison to the LTM predictions. For the glass beads, the A_{aw}-S_w relationships predicted by the LTM (using the α and n values provided by the Benson PTF) are very similar to those provided by the XMT measurements. Both methods practically predict the same maximum interfacial areas (i.e., the endpoint A_{aw} prediction at $S_w = 0$), which are estimated using the smooth surface *GSA* values represented in Table 1. For the fine glass bead media, the LTM prediction deviates upward from the XMT results with increasing separation as S_w approaches S_r, which results from the lower value of α provided by the Benson PTF in response to the decrease in particle size. Costanza-Robinson et al. (2008) describe the XMT results as being less accurate for the fine bead media due to the poor image segmentation quality that resulted in only a qualitative estimation of A_{aw} values. However, both methods provided reasonably similar A_{aw}-S_w relationships. This is true for the highly uniform and largely spherical Accusand media as well (e.g., particle roundness = 0.8, sphericity = 0.8–0.9 (Schroth et al., 1996; Hamamoto et al., 2016). The observed similarity in A_{aw} values implies that both methods are characterizing the same effective interfacial areas for these uniform, spherical, and smooth porous media.

For the glass bead mixture, the A_{aw} values predicted by the LTM are overall greater than those by the XMT method. In this case, it appears that the XMT may be underestimating A_{aw} values for this mixture. Costanza-Robinson et al. (2008) noted that pore-water within the XMT-imaged bead mixture sample was observed to be non-uniformly distributed within the images analyzed due to preferential capillary filling of small pores associated with the fine bead fraction (i.e., a presented imaged section for the bead mixture sample used in the analysis shows an area of water associated with the fine bead fraction that encompasses roughly a third of the image area); whereas pore-water was

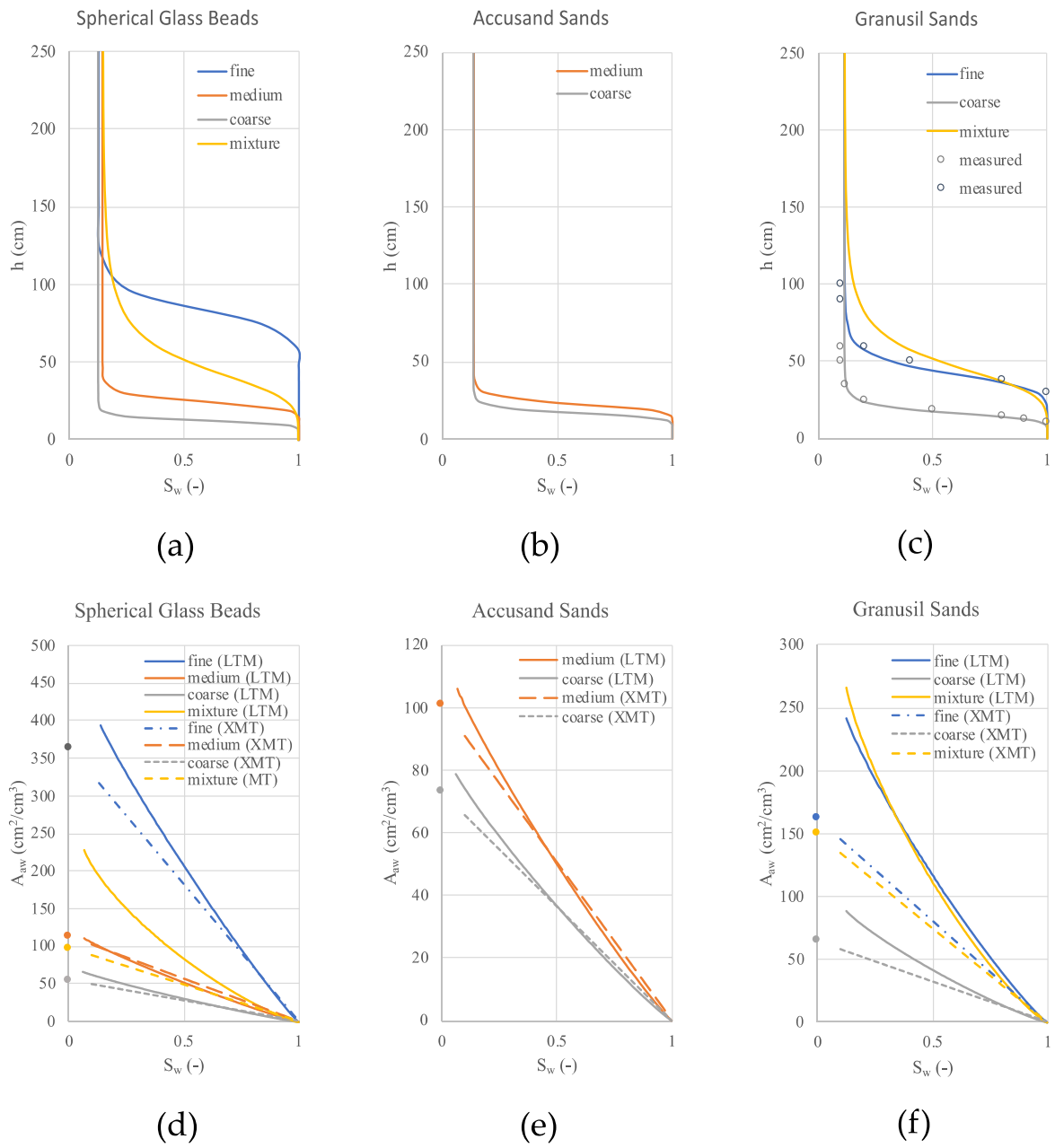

Fig. 1. SWRCs (a-c) and associated A_{aw}-S_w relationships (d-f) for porous media used in this evaluation. Linear dashed A_{aw}-S_w relationships are those estimated and reported by Costanza-Robinson et al. (2008) using XMT methods. Solid lines are the LTM predictions. Filled symbols are the calculated GSA values for the media. Open symbols are measured data from Sakaki and Illangasekare (2007).

observed to be homogeneously distributed in the uniform bead media sample images. The presence of heterogeneously distributed water in the non-uniform sample is not surprising in and of itself. However, it calls into question whether the A_{aw} value estimated from this sampled image would be reproducible for another sampling at the same moisture condition and at the scale of measurement. This issue also raises the question as to whether the sample scale for the XMT measurement meets the requirement of a REV for this non-uniformly sized glass bead mixture. Complications related to the REVs and XMT A_{aw} calculations for non-uniform media have been recently documented (Costanza-Robinson et al., 2011; Wang et al., 2019). The increased slope of the LTM-predicted A_{aw}-S_w relationship is the result of the reduction in the α parameter provided for this non-uniform bead mixture ($C_u = 4.6$). For the VG equation, parameters vary systematically with the median particle size; α should decrease as the median particle size decreases and as the breadth of the particle size distribution increases, and n should decrease as the breadth of the particle size distribution increases (Benson et al., 2014).

A_{aw} values for the Granusil sands predicted by the LTM, again using α and n values provided by the Benson PTF, were also overall larger than those for the XMT results for both the fine- and coarse-grained fractions and the mixture. However, the reason for the difference in A_{aw} values, in this case, does not appear to be related to the heterogeneous pore-water distribution issues observed for the glass bead mixture. The pore-water distribution in the XMT images presented by Costanza-Robinson et al. (2008) appears to be more uniform within the Granusil sands in all cases. Here, we interpret the differences between XMT and LTM estimates as being related to the Granusil sands' angularity (roundness = 0.2; sphericity = 0.7) (Hamamoto et al., 2016) and increased roughness of the particle surfaces. As noted by Costanza-Robinson et al. (2008), the

XMT method uses surface smoothing algorithms to minimize imaging artifacts as a part of estimating A_{aw} values, which removes micro-scale surface topographic heterogeneity (i.e., surface roughness) of media particles. XMT, therefore, provides smoothed-surface estimates of A_{aw} that compare well with GSA values. Conversely, previous research has shown that particle surface roughness is captured in the results of media fluid retention curves (Dullien et al., 1989; Zheng et al., 2015). With respect to the SWRC, the angularity of the Granusil media allows greater packing density than for more rounded sands of the same particle size, which results in an smaller pores and subsequently an increased air-entry pressure for this media during drainage, with a corresponding reduction in the VG α parameter. Likewise, an increased media surface roughness would also manifest in a reduced α parameter. The net effect of these media characteristics would then be an increased slope of the A_{aw}-S_w relationship predicted by the LTM than would be measured by XMT, as demonstrated in Fig. 1f. Given the agreement between measured data and the predicted SWRCs shown in Fig. 1c, the Benton PTF appears to be providing VG parameters that are indirectly, but appropriately, accounting for the effects of the angularity and surface roughness of the Granusil sands.

3.4. Comparing XMT and LTM predictions for natural Sandy soils

The majority of the existing literature data relating to estimating A_{aw} for unsaturated porous media is limited to some model sands (i.e, constructed using well-sorted sand fractions) and a few sandy soils (i.e., the Vinton and Hayhook soils described previously). Relevant data collected for these sands are also presented in Table 1. To our knowledge, when this paper was prepared, XMT measurement data had been only reported for the Vinton soil (Brusseau et al., 2006). The LTM was applied using VG parameters derived from the Benson PTF, published measured parameters, and those derived from the Rosetta model as described in Section 2.2. For the Rosetta model, the textural classification of the Vinton soil was 97% sand, 1.8% Silt, 1.2% clay, and ρ_d= 1.46 (Costanza-Robinson, 2001; Peng and Brusseau, 2005). Likewise, the Hayhook soil was classified as containing 86% sand, 4.7% silt, and 8.8% clay (Torrens et al., 1998), with ρ_b= 1.64 g cm^{-3} (Peng and Brusseau, 2005).

The A_{aw}-S_w relationships developed for the Vinton and Hayhook soils (Fig. 2) demonstrate the dependence of the LTM prediction on the selection of α and n provided by different parameter estimation methods selected. Note that for both soils, the Benson PTF predicts lower α values (Table 1), which translates to a higher air-entry pressure for the SWRCs and increased A_{aw} values than those predicted when using the other methods at the same S_w (Fig. 2). Additionally, the Benson PTF provides values of n that are larger than those derived using the other methods. In comparing the SWRCs derived from the Benson PTF and the measured VG parameters for these natural sandy soils, the Benson PTF appears to overestimate the moisture retention contribution of the fines fraction at higher S_w. As noted by Benson et al. (2014), the PTF was developed using sands for which the fine fraction (i.e., particles <0.075 mm) was removed. Therefore, exclusion of the fines fraction appears to be weighting the effect of C_u more heavily on the predicted value of α than on the value of n when fines exist in the sample and for $C_u > 2$.

To correct this, the following simple modification to the Benson PTF was made:

$$N_\alpha = 0.99{C_u}^{-0.2}, \text{and} \quad (9)$$

$$N_n(C_u > 2.2) = -0.0033C_u + 0.279 \quad (10)$$

Applying these corrected equations, the resulting values of α for the Vinton and Hayhook soils (drying curve) become 0.026 cm^{-1} and 0.02 cm^{-1}, respectively. Likewise, the n values for these same soils become 3.53 and 2.91, respectively. As shown in Fig. 2, using these corrected parameters results in SWRCs and A_{aw}-S_w relationships that closely match those derived from the measured VG parameters. This is particularly the case for the Hayhook soil, where the fines fraction is more considerable.

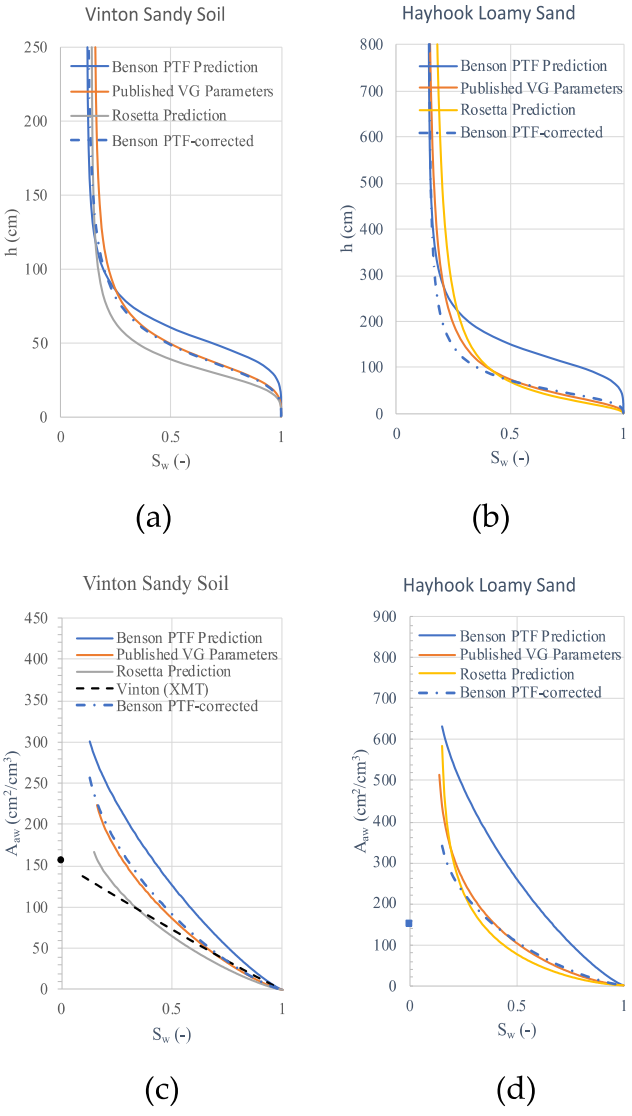

Fig. 2. SWRCs (a-b) and associated A_{aw}-S_w relationships (c-d) for natural sandy soils. Filled symbols are the calculated GSA values for the media.

While additional measured A_{aw}-S_w relationships for natural soils would be needed to validate the corrections made here to the Benson PTF, these results indicate that it is possible that a simple correction to the PTF could render it more useful for estimating A_{aw}-S_w relationships by the LTM for natural sandy soils containing fines. This discussion highlights the importance of obtaining SWRCs that are most representative of the vadose zone soils in question when using the LTM approach to derive A_{aw}-S_w relationships. It is additionally important to note that applying the LTM approach is not limited to using VG-based models to characterize soil-water retention characteristics. Other models, including the Brooks-Corey model (e.g., Oostrom et al., 2001), can also be used.

3.5. Comparisons with aqueous tracer-based methods

In addition to the XMT methods, air-water interfacial adsorbing tracers have also been used to estimate A_{aw}. These have included both gas-phase tracers (GT) and aqueous-phase tracers (AT). The GT methods have been shown to provide A_{aw} values that are significantly greater than those provided by aqueous tracers, with A_{aw} approaching the area of the media determined by BET measurement as $S_w \rightarrow 0$ (Peng and Brusseau, 2012). The XMT methods provide maximal A_{aw} values that closely match the GSA for uniform media with smooth surface areas. The

fact that the A_{aw}-S_w relationships provided by the LTM closely match those of the XMT methods for the uniform smooth and spherical media categories implies that the LTM is a good predictor of the interfacial area associated with natural pore-water drainage and imbibition (Leverett, 1941; Kibbey and Chen, 2012). The AT methods have also been shown to provide A_{aw} values that were consistent with XMT results for smooth glass bead media (e.g., El Ouni et al., 2021), indicating both methods are quantifying the same interfacial areas (see, e.g., Fig. 3 – glass bead comparison). However, for some model sands and natural soils, the AT methods have provided A_{aw} values that are greater than those measured by XMT, with maximal values falling between those measured by the GT and XMT methods.

As demonstrated in Fig. 3, the XMT and LTM methods provide lower A_{aw} values than the AT methods for the Accusand media and Vinton soil. The two AT methods shown represent the results of both advecting aqueous tracer (A-AT) methods and those determined by mass balance

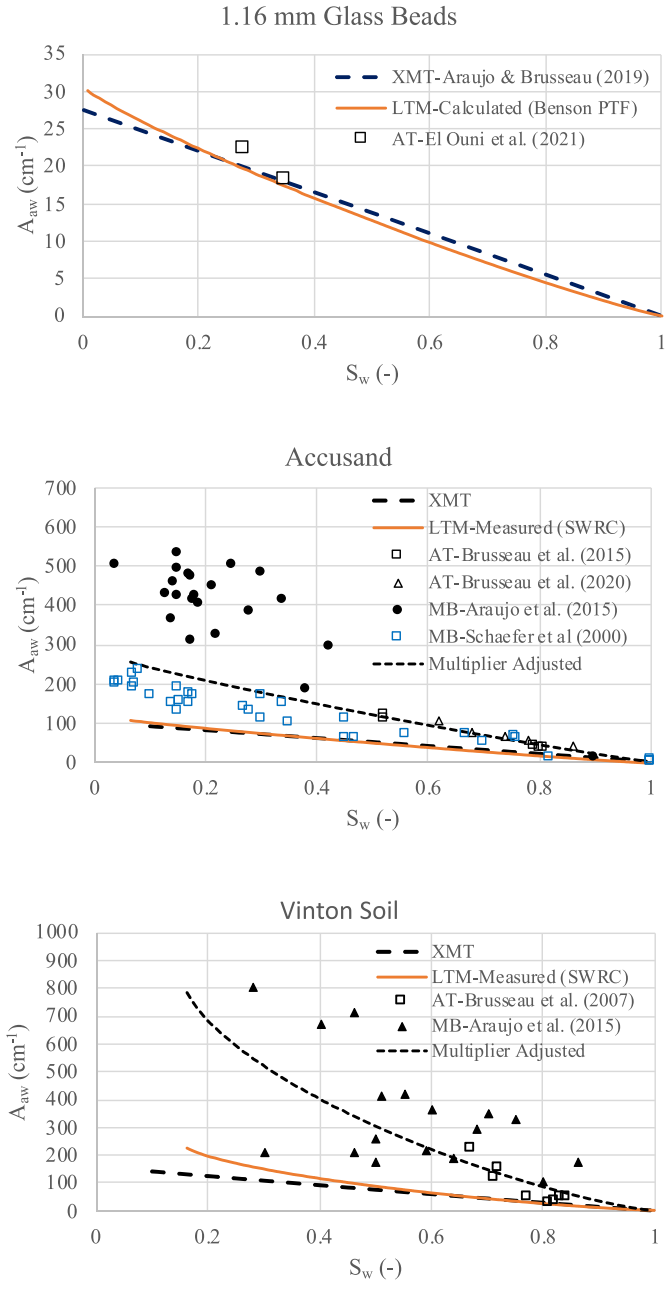

Fig. 3. Comparison of XMT, LTM, and AT derived A_{aw}-S_w relationships for porous media with different degrees of surface roughness.

(MB) methods (Schaefer et al., 2000; Araujo et al., 2015). For the Accusand (40/50 grade, $d_{50} = 0.35$ mm sand in all cases), the A-AT data presented in Fig. 3 was derived from the published results of two separate experiments using different interfacial-adsorbing tracers (including one in which the PFAS perfluorodecanoic acid (PFDA) was used as a tracer) and performed under different flow and input concentration conditions (Brusseau et al., 2015; Brusseau et al., 2020). These A-AT experiments provide similar A_{aw}-S_w relationships (Fig. 3). However, the extent to which these A-AT experiments can characterize A_{aw}-S_w relationships is limited to the higher range of S_w (e.g., $S_w > 0.5$), given the difficulty in maintaining a steady and uniform flow condition at lower S_w for these types of experiments.

The MB method results derived from the published results of Schaefer et al. (2000) generally exhibit the same linear trending A_{aw}-S_w relationship for the Accusand media as that provided by the A-AT results. The MB method is considered a viable approach to quantifying A_{aw} at lower S_w conditions because it does not rely on flow, but rather on the equilibrium distribution of tracer between the interface and other environmental compartments. However, the approach does result in more scatter in the A_{aw}-S_w data. Brusseau (2020) noted that the scatter in the MB method is a potential limitation of the method. The results provided by Araujo et al. (2015), also presented in Fig. 3 for the same Accusand sand, exhibit considerably more scatter in the data, with A_{aw} values that are considerably greater than those provided by Schaefer et al. (2000). While it might be tempting to plot a line through the cloud of datapoints, this approach is not tenable given that this ignores the results of Schaefer et al. (2000), who used a similar approach and the same sand. Results similar to Schaefer et al. (2000) were reported by Chen and Kibbey (2006) for F110 Ottawa sand undergoing multiple draining cycles using sodium octylbenzene sulfonate as a surface-active tracer and an alternative measurement method. The uncertainty in the MB-measured A_{aw} values for the Vinton sand is even more significant. As a result, going forward, we will rely on the A-AT dataset as a basis for comparing results.

The disparity between the XMT data and the A-AT A_{aw} values has been attributed to the ability of the tracer to access the interfacial area associated with micro-scale rough particle surfaces that is too small to be resolved by the XMT methods (e.g., Brusseau et al., 2006; Brusseau et al., 2007; McDonald et al., 2016). That is, the A-AT method is characterizing both A_{aw} associated with capillary-held pendular water and some additional fraction of the A_{aw} associated with pore surface films of water that is impacted by the microscale roughness of the surface. However, the effect of surface roughness on the magnitude of the total A_{aw} existing within an unsaturated porous media is a topic of continuing research and debate.

For example, using stereoscopic scanning electron microscopy (SEM) methods and surface configuration modeling, Kibbey (2013) demonstrated that surface-associated water remains held to the surface via capillary tension, which results in a significantly smoother air-water interfacial surface than that of the underlying solid surface. As a result, the impact of surface roughness on the A_{aw} was shown to be greatly minimized during drainage for capillary pressure heads less than −100 cm. A capillary pressure head of −100 cm or less would be needed to drain most of the media included in this evaluation to residual saturation, including the Vinton soil. This would suggest that these same media should present a smooth air-water interface for these surfaces under normal drainage, with the magnitude of A_{aw} associated with these wetted surfaces being well-characterized by the XMT methods. Further, if water associated with surface roughness is held by capillarity, the presence of this water should be represented in the SWRC, as demonstrated in the literature (e.g., Dullien et al., 1989; Zheng et al., 2015). Therefore, the LTM A_{aw}-S_w relationship predictions should be additionally representative. This was also the position of Kibbey and Chen (2012), who contend that the LTM provides the maximum possible area formed during natural drainage.

The utility of the A-AT method to characterize interfacial areas was

further challenged by Kibbey and Chen (2012), who used pore network modeling to demonstrate that neither diffusion nor head-driven flow was sufficient to allow access to surface films (i.e., those presumed to be associated with the increased A_{aw} for A-AT). These authors also suggested that, in the absence of additional experimental artifacts, surface charge or surface tension gradient-driven advection would be needed for surface-active tracers to access these surface films. This possibility was examined by Costanza-Robinson and Henry (2017), who performed a numerical modeling study to demonstrate the impact of surface-tension induced flow potentially providing artificially enhanced A_{aw} values determined by the A-AT methods. However, given the reported reproducibility of the A-AT results for experiments using different tracers at different concentrations (Brusseau et al., 2015; Brusseau et al., 2020), and the recent method validity evaluation provided by El Ouni et al. (2021), who demonstrated that bulk surface-tension induced flow and other potential experimental artifacts were not relevant, it is difficult to ignore the A-AT measurements. In their modeling evaluation, Kibbey and Chen (2012) did not include the effects of microscopic surface roughness, an omission that was thereafter addressed by Jiang et al. (2019), who showed that including surface roughness resulted in the same monotonic increases in A_{aw} values at high to moderate S_w values and exponentially increasing A_{aw} values at low S_w, as observed by the GT methods.

However, while Jiang et al. (2019) demonstrate that these higher A_{aw} values could be caused by surface roughness at lower S_w and that the resulting A_{aw}-S_w relationships can be made to match measured data, they did not extend this evaluation to include a reason as to how these surface-active tracers would contact this additional surface roughness-associated interfacial area during aqueous transport under an assumed uniform and constant soil moisture condition. Kibbey (2013) demonstrated a thicker layer of water associated with rough surfaces and suggested that diffusion of solutes within this thicker capillary-held surface-associated water may be possible, wherein diffusive rates may increase by roughly two orders of magnitude due to the resulting larger cross-sectional areas for diffusion. This diffusive mechanism could, in turn, allow surface-active tracers to contact a larger portion of the total interfacial area, thus yielding larger AT-measured A_{aw} values than would be the case for a smooth surfaced media. Diffusion of solutes into and out of these thickened surface-associated water films could have contributed to the rate-limited diffusional mass transfer characterized in the column experiments presented by Brusseau (2020) for the water-unsaturated transport of non-reactive and surface-active solutes between advective and non-advective domains. Therefore, it is possible that this thickened-film diffusive mass transfer could be contributing to the disparity between the A_{aw} values provided by the A-AT and LTM.

Alternatively, and despite the convincing discussions provided by El Ouni et al. (2021) and Brusseau et al. (2020), it seems likely that a surface-active tracer adsorbing to an air-water interface would impact the magnitude of the interfacial area it is accesing for measurement. The A-AT method is physically a chromatographic technique that assumes that the stationary phase (i.e., the air-water interface in this case) has a constant area spatially and temporally during the test. While this can be reliably assumed to be the case for solid adsorbent media, fluid-fluid interfacial areas are generally not as stable. In the context of the previous discussion, perturbations in the surface charge or surface pressure/tension of the air-water interface due to interfacial adsorption, even at a very low concentration, could still disrupt cohesive forces between water molecules at the interface enough to modify the configuration of water films associated with rough surfaces. These perturbations might not be significant enough to drain interparticle pendular water but could cause a localized displacement of water films, or deformation of water film surfaces, that could manifest as a localized increase in A_{aw} as the pulse of the surface-active tracer moves through the porous medium. For the A-AT method, this increased interfacial area would increase tracer retention and ultimately provide a larger measured A_{aw} value than would be predicted by the LTM at the same S_w. It is unlikely that this type of film water displacement would be observable at the column or continuum scale. In this context, the A-AT method would then provide an effective A_{aw} for these amphiphilic surface-active tracers and not necessarily the true A_{aw} for the unsaturated medium, which has been reported to be provided by the LTM (Kibbey and Chen, 2012). As shown in Fig. 3, when the surface roughness is absent, both the A-AT and LTM methods predict the same A_{aw}-S_w relationship, which strengthens the argument that surface roughness is a key factor in the A-AT results.

3.6. Modifying the LTM to include tracer-accessible area

While the causal mechanisms are not fully understood, the experimental results presented in the literature suggest that aqueous interfacial tracers are measuring higher A_{aw} values than those predicted by the LTM, and the discrepancy appears to be related to changes in the degree of surface roughness of the porous media (see Fig. 3, Table 1). This is not necessarily problematic for PFAS because these chemicals, like the tracers used for the A-AT method, are also surface-active and amphiphilic. Therefore, A_{aw}-S_w relationships that are representative of surface-active solutes are needed for predicting the retention contribution of air-water interfacial adsorption during transport. What is problematic is that continuum models, like the LTM, do not account for the observed effects of surface-active solutes and surface roughness. The following modification to the LTM is proposed to correct this discrepancy.

The modification applies a direct surface roughness multiplier (SRM) to the A_{aw}-S_w relationship provided by the LTM (recall Eq. (1)). This simple approach allows the LTM prediction to continue to include the effects of particle size, uniformity, and differences in packing density as it relates to particle angularity – as governed by the SWRC for capillary water – while also capturing the contributive effects of surface roughness on the magnitude of A_{aw} at a given moisture condition. Using the A-AT data as the benchmark A_{aw}-S_w relationship in this application, the SRM values needed to match the A-AT A_{aw}-S_w relationship for the Accusand and Vinton soil examples are 2.4 and 3.3, respectively.

The results of applying the SRM to the Accusand and Vinton soil A_{aw}-S_w relationships are also presented in Fig. 3. Note that the SRM-adjusted LTM result for the Accusand media maintains a more linear trending A_{aw}-S_w relationship with decreasing S_w, owing to the particle size uniformity of the model sand. This result is consistent with the MB tracer results of Schaefer et al. (2000), the sphericity and uniformity of the sand, and the low soil surface roughness factor (SRF) calculated for this sand (i.e., SRF = 18 for the medium Accusand as in Table 1). In contrast, the SRM-adjusted LTM result for the natural Vinton soil exhibits a more distinct non-linearly increasing A_{aw}-S_w relationship with decreasing S_w, consistent with the increased fines fraction, less uniform particle-size distribution, and factor of 18.6 increase in the SRF for this soil as compared to the model sand. It is important also to note that this approach does not attempt to characterize the significantly increased A_{aw} values observed by the GT results at lower S_w. In keeping with the limitations of the LTM (Leverett, 1941; Bradford and Leij, 1997), the low S_w endpoint of the SRM-adjusted A_{aw}-S_w relationships are truncated at the residual saturation for a given porous media, which is appropriate for unsaturated transport under aqueous advection (i.e., advective flow is not expected when water content is below residual saturation).

To guide the selection of SRM values for other natural soils, a soil surface roughness factor (SRF), initially proposed by Wenzel (1936) and applied more recently by others when evaluating A_{aw}-S_w relationships (e.g., Brusseau et al., 2007; Costanza-Robinson et al., 2008; Jiang et al., 2019), was used. As additionally described in Table 1, the SRF is redefined here as:

$$SRF = N_2\ BET\ Area/_{GSA} \tag{11}$$

where GSA is the smooth geometric surface of the soil calculated using Eq. (4). Properties for 21 Arizona soils were collected from the literature

(i.e., Arthur et al., 2012; Ghanbarian et al., 2021). This data is provided in Table 2. In addition to the SRF, Ghanbarian et al. (2021) provided measured soil surface fractal dimensions (D_s) for each of these same soils from water retention curves that were used to additionally characterize soil surface roughness. D_s is an index of the topographical complexity of soil surfaces as it relates to scale and characterizes the change in surface roughness between soil textural classifications. As these D_s values were derived from water retention data, they are representative of the degree of surface roughness at the continuum scale, in keeping with the LTM predictions. The three-dimensional D_s values vary between 2 and 3 (Pfeifer et al., 1983; Wang et al., 2005). A value of 2 indicates a smooth surface, and a value of 3 corresponds to an extremely rough soil particle surface. As observed in Table 2, D_s values generally increase with increasing clay content. D_s values ranging between 2.09 and 2.3 have been documented for model sands similar to those described in Table 1 (Avnir et al., 1985; Yang et al., 2016).

The D_s values were used to approximate the rate of change of surface roughness for these soils relative to their corresponding SRF values (as shown in Fig. 4a). This slope was then used, in concert with the SRFs and SRMs determined for the Accusand and Vinton soil, to provide data with which to develop an empirical model to estimate SRM values for soils of varied texture. A Langmuir-like equation was used to fit the Accusand and Vinton data and the slope of the D_s-SRF relationship was used to scale the extrapolation of the model with increasing SRF. The results of this work are presented in Fig. 4b. Note that the proposed SRM-SRF model is scaled such that SRM = 1 when SRF = 1, which defines a smooth surface condition consistent with the A_{aw}-S_w results for the glass bead case shown in Fig. 3. Additionally, in keeping with the trend provided by the D_s-SRF relationship, SRM values do not exceed a value of 3.5 as SRF values increase.

Unfortunately, no additional A_{aw}-S_w data for natural soils was found in the published literature, precluding further validation of the proposed SRF-SRM model. This lack of A_{aw}-S_w relationship data presents a significant data gap for this area of research and is problematic with respect to assessing the fate and transport of surface-active contaminants, like PFAS, as there is a growing need to model PFAS transport in vadose zones comprised of soils of varied textural classification. Strictly, the SRF-SRM model would be most applicable to sands and predominantly sandy soils similar to those described herein. On the other hand, for soils with broad particle size distributions (e.g., loams and clayey soils), it is possible that the effects of surface roughness on the A_{aw}-S_w relationship could be overwhelmed by the contributions of interparticle capillary effects, obviating the need for correcting the LTM prediction. Therefore, more research is needed to determine the importance of surface roughness on A_{aw} values for a wider variety of natural soils and sediments, particularly with respect to supporting site-scale modeling. However, the proposed SRF-SRM model provides a practical first-approximation method that incorporates the effects of surface roughness on A_{aw} estimates provided by the LTM, where the SRM can be estimated from common soil textural classification measurements (i.e., the BET specific surface area of the soil sample and the median particle size, or d_{50}).

Examples of LTM-predicted A_{aw}-S_w relationships are compared in Fig. 5 to their corresponding SRM-corrected relationships for a few sandy soils and a loam selected from Table 2. Textural data from Table 2 was used as input to the Rosetta model (described previously) to provide VG parameters and generate SWRCs that were then used to generate LTM predictions. Texturally, the sand and loamy sand results are most consistent with the Vinton soil and the Hayhook soil, as are the predicted A_{aw}-S_w relationships. Regarding the loamy sand predictions, the SRM-adjusted A_{aw}-S_w relationship closely matches that of the SRM-adjusted sand results until S_w= 0.5. A_{aw} values increase considerably thereafter, representing the effect of surface roughness on the magnitude of the A_{aw} with increased pore-water drainage at the continuum scale. As the fines content of the soil increase, predicted A_{aw} values increase. For the sandy loam and loam soils, predicted A_{aw}values are roughly a factor of 10 greater than those of the sand and loamy sand as S_w falls below 0.2. In these cases, it is important to consider that field capacities for a typical sandy loam and loam soil range between θ = 0.18–0.28 and θ = 0.25–0.32, respectively (or S_w = 0.47–0.73 and S_w = 0.6–0.76, respectively). Under typical field conditions, these soils should retain enough moisture to limit the magnitude of the A_{aw} and the contribution of AWI adsorption during PFAS transport. However, this would not necessarily hold true for soils positioned at the ground surface in an arid environment, where much lower water saturations could be achieved via evaporative losses, where A_{aw} values could be large, and PFAS could be significantly retained within the shallow vadose zone as a result.

3.7. The significance of the A_{aw}-S_w relationship on transport

The potential effect of this A_{aw}variability on PFAS retardation factors (R) is demonstrated for PFOS, a representative PFAS, and is presented in Fig. 6. R-values were calculated using the following equation:

Table 2
Soil properties data used to modify LTM prediction.

Arizona soils	SSA_{BET}[a] (cm^{-1})	Category	%sand/silt/clay	porosity	d_{50} (mm)	GSA (cm^{-1})	SRF	SRM	D_s (−)
1	22,800	sand	91/7/2	0.36	0.17	22.6	1009	3.43	2.65
2	16,800	sand	96/3/1	0.36	0.17	22.6	744	3.41	2.68
3	37,500	loamy sand	81/14/5	0.38	0.135	27.6	1361	3.45	2.71
4	93,750	sandy loam	74/18/8	0.38	0.098	38.0	2470	3.47	2.68
5	76,500	loamy sand	80/14/6	0.37	0.135	28.0	2732	3.47	2.70
6	111,000	sandy loam	67/25/8	0.39	0.098	37.3	2972	3.48	2.71
7	296,100	sandy loam	71/16/13	0.39	0.06	61.0	4854	4.31	2.76
8	107,550	sandy loam	59/32/9	0.4	0.098	36.7	2928	4.11	2.69
9	149,400	sandy clay loam	53/26/21	0.43	0.07	48.9	3058	4.13	2.74
10	150,750	silt loam	22/53/25	0.46	0.027	120.0	1256	3.78	2.74
11	222,900	loam	37/46/17	0.42	0.035	99.4	2242	4.01	2.70
12	466,800	loam	39/40/21	0.4	0.035	102.9	4538	4.28	2.76
13	392,550	sandy clay loam	66/15/27	0.4	0.035	102.9	3816	4.21	2.78
14	317,700	sandy clay loam	58/15/27	0.42	0.027	128.9	2465	4.04	2.81
15	525,600	sandy clay loam	51/22/27	0.43	0.027	126.7	4149	4.25	2.81
16	436,050	silt loam	4/73/23	0.45	0.027	122.2	3568	4.19	2.76
17	397,050	clay loam	26/45/29	0.43	0.018	190.0	2090	3.98	2.78
18	535,200	silty clay	9/40/51	0.43	0.006	570.0	939	3.67	2.81
19	781,500	clay	29/19/52	0.45	0.006	550.0	1421	3.83	2.87
20	570,750	sandy clay loam	49/21/30	0.41	0.027	131.1	4353	4.27	2.83
21	92,250	sandy loam	71/20/9	0.38	0.098	38.0	2430	4.04	2.70

[a] Reported specific surface area from N_2/BET. d_{50} values from Dosskey et al. (2006). D_s is the surface fractal dimension (Ghanbarian et al., 2021).

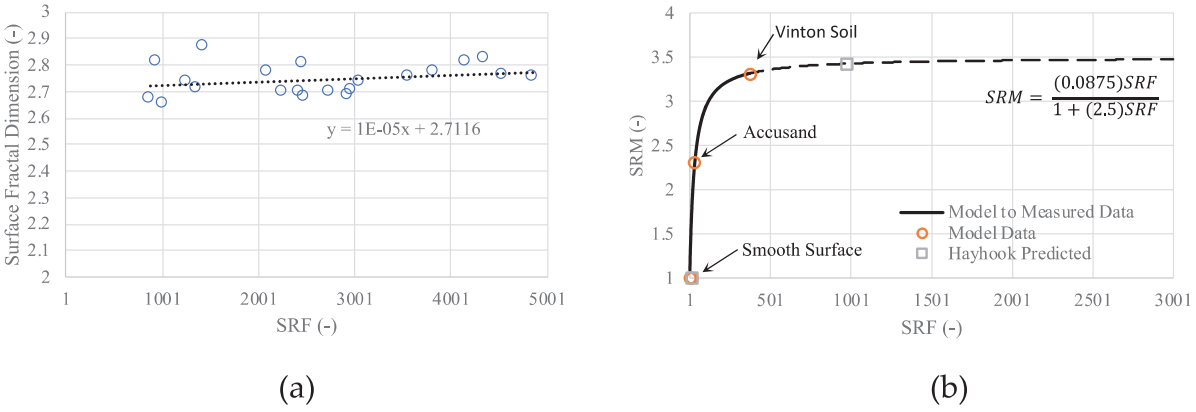

Fig. 4. Data used to develop an empirical model to estimate SRM values: (a) the rate of change of D_s with increasing SRF, and (b) model fit to available SRM-SRF data. Dashed line in 4b indicates extrapolation of model prediction to higher SRF based on the slope of the surface fractal dimension in 4a.

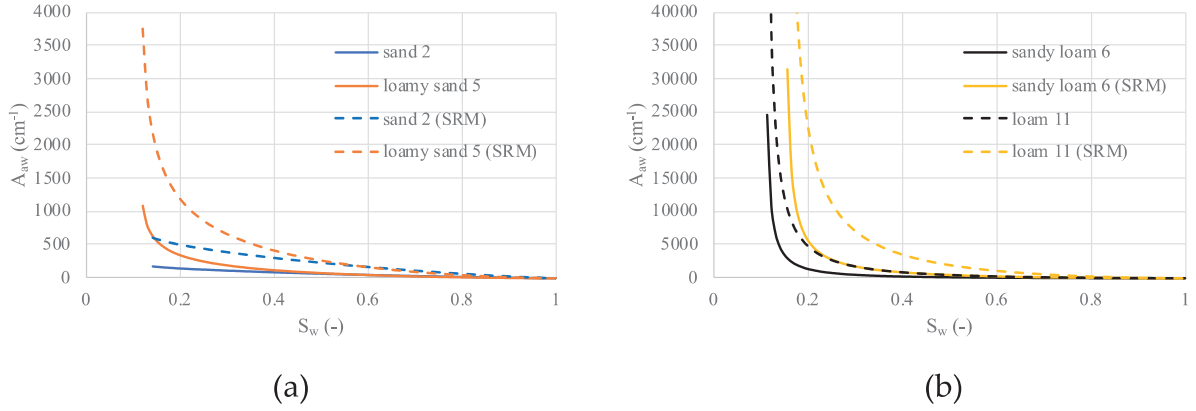

Fig. 5. LTM and SRM-adjusted LTM predictions of the A_{aw}-S_w relationships for media selected from Table 2: (a) sand 2 and loamy sand 5, (b) sandy loam 6 and loam 11.

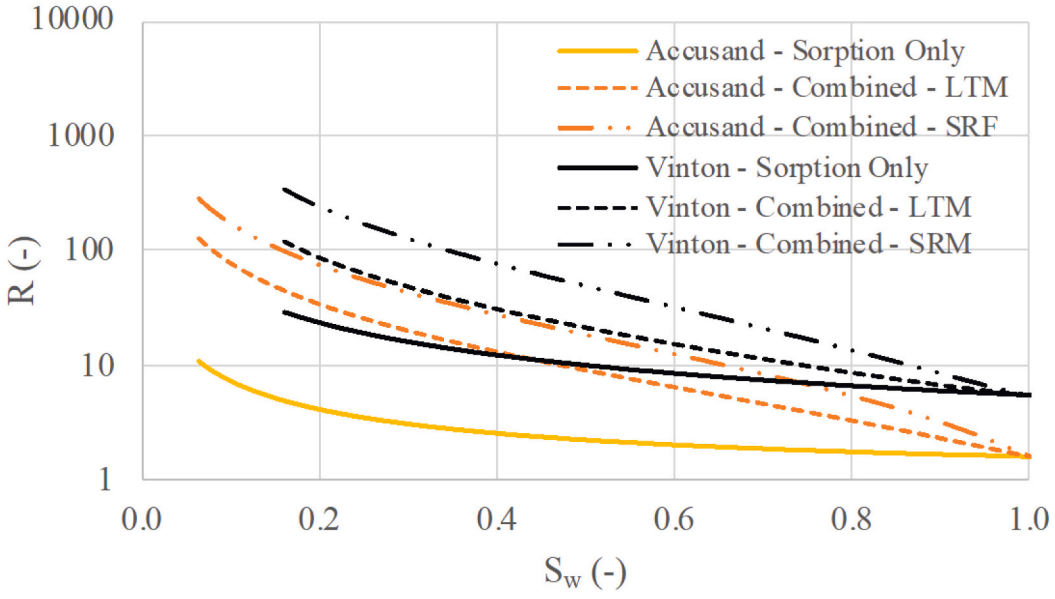

Fig. 6. Calculated ranges for PFOS retardation with changing S_w for the Accusand media and the Vinton soil. Combined refers to the inclusion of solid-phase sorption and AWI adsorption. LTM refers to the use of the LTM model (Eq. (1)) and SRM is the LTM model result when the SRM is applied.

$$R = 1 + \frac{\rho_b K_d}{\theta} + \frac{k_{aw} A_{aw}}{\theta} \quad (12)$$

where ρ_b is the soil bulk density (M/L^3), K_d is the solid-phase sorption coefficient (L^3/M^1), k_{aw} is the air-water adsorption coefficient (L), and $\theta = S_w n$. As presented, Eq. (12) assumes linear solid-phase sorption and that sorption and air-water interfacial adsorption are the only sources of retention. Sorption coefficients (K_d) were 0.16 and 1.2 cm^3/g for the Accusand and Vinton soil, respectively, and were derived from the linear model fit to the data presented by van Glubt et al. (2021) for solute concentrations <1 mg/L. Other parameters used in these calculations were: ρ_b= 1.5 g/cm^3 and k_{aw}= 0.026 cm. The results of these calculations (Fig. 6) demonstrate not only the variability in PFOS retention, but also the importance of using the appropriate A_{aw}-S_w relationship when surface-active solutes are being considered, because vadose-zone PFAS retention could be greatly misrepresented.

Finally, it is important to note that all A_{aw}-S_w relationships used in this work were derived from data representing drainage conditions. The magnitude of A_{aw} values in the vadose zone will be impacted by transient cycles of drainage and imbibition (wetting) during natural infiltration events. While Leverett (1941) demonstrates the LTM could be applied to both drainage and imbibition conditions, characterized by separate SWRCs and potentially providing different A_{aw}-S_w relationships for each condition, the validity of this application with respect to the transport of PFAS has not been. Using A-AT methods and the Vinton soil, Brusseau et al. (2007) observed that A_{aw}-S_w relationships measured under both drainage and imbibition conditions were similar and cited the importance of surface roughness associated water films for the similarity in measured A_{aw} values. Schaefer et al. (2000) also observed similar A_{aw}-S_w relationships under drainage and imbibition conditions using MB methods. However, both studies utilized a surface-active tracer (i.e., sodium dodecyl benzenesulfonate) at concentrations that would promote interfacial tension reduction and could have altered the moisture retention characteristics that would have been observed for water without surfactant. Therefore, additional research is needed on this topic.

4. Conclusions

When performing calculations or numerical simulations of the fate and transport of PFAS and other surface-active solutes in the vadose zone, and accurate A_{aw}-S_w relationship is needed. Most research has focused on accurate characterization of interfacial adsorption coefficients and the associated concentration dependence. However, capturing changes in the A_{aw}-S_w relationship relationship that result from changes in soil texture is equally important. Indeed, accurate determination of the A_{aw}-S_w relationship is arguably more important when one considers the challenges in characterizing heterogeneity at both the pore- and continuum scale and its relationship to the SWRC and A_{aw}-S_w relationship. In this work, the well-known LTM model is compared to two methods for the determination of the A_{aw}-S_w relationship: microtomography and aqueous tracer methods. The LTM model is favored here due to its simplicity, and because it represents the change in the magnitude of the A_{aw} with changes in S_w at the continuum scale, consistent with practical methods used to model PFAS transport (i.e., continuum mechanics behind the SWRC and the application of the Richards equation for unsaturated flow). In addition, the LTM method is less time-consuming and expensive, yet appropriately captures the effects of soil particle size, uniformity in the particle size distribution, and differences in packing density on the A_{aw}-S_w relationship.

The XMT, the A-AT method, and the LTM were found to provide very similar A_{aw}-S_w relationships when the porous media surface is smooth (i.e., glass beads), suggesting each method characterizes the same effective interfacial area in these cases. However, both the LTM and A-AT methods provide larger A_{aw} values than measured by the XMT method for non-uniform, increasingly angular media, or when the surfaces of the media become rougher (as characterized by the proposed SRF). The A-AT method was shown to provide A_{aw} values that are consistently greater than both the XMT and LTM results for a given S_w, with the degree of difference increasing with increased surface roughness, consistent with the conclusions drawn from literature sources wherein much of the A-AT data was obtained.

The A-AT method utilizes surface-active solutes as tracers to characterize A_{aw} at the continuum scale in porous media columns. These tracers appear to be sampling portions of the air-water interface that are not represented by either the LTM prediction or XLM measurements. While the exact mechanism for this disparity is uncertain, it appears that the degree of microscale surface roughness is a dominant contributing factor. Because the AT method uses tracers that are surface-active, and the contaminants of interest in this work are also surface-active, it is reasonable to conclude the tracers themselves may influence the interfacial area. Thus, the A-AT data provides the most representative A_{aw} values for surface-active solutes like PFAS. In addition, the LTM (and similar thermodynamic methods) likely provide a true measure of the A_{aw} under natural drainage conditions, a conclusion based on the presentations of Kibbey and Chen (2012) and Kibbey (2013) and on the similarity in predicted A_{aw}-S_w relationships when media surfaces are smooth.

Using the literature-derived A-AT measured A_{aw}-S_w relationships as a benchmark for surface-active tracers, the LTM prediction was modified to include the effects of surface roughness on the predicted A_{aw}-S_w relationship by applying a direct multiplier to the LTM prediction to account for surface roughness (i.e., the SRM). An empirical model was developed using the measured data to estimate the magnitude of the SRM with changes in calculated SRF values as soil textural classifications change. Because this empirical model was developed from a limited dataset, it should be considered to provide only first-order estimates; additional measured A_{aw}-S_w relationships for a wider variety of soil textures are needed for a more robust test of this empirical model. However, in the absence of this additional data, the approach provides a practical method for calculating or simulating PFAS mass transport in the vadose zone and accounting for the effects of surface roughness on A_{aw}-S_w relationships.

Finally, because the representativeness of the A_{aw}-S_w relationships predicted by the LTM depends on the representativeness of the SWRC used, methods of estimating VG parameters that define the SWRCs were compared. The accuracy of the Rosetta model was found to improve when fines (e.g., particles <0.0075 mm) are present in the soil. For non-uniform sandy soils without fines, the Benson PTF, which corrects predictions for changes in the uniformity of porous media particles, was shown to best match measured SWRCs for the sands presented in this work. The Benson PTF was also modified to account for the presence of fines, which greatly improved the accuracy of the A_{aw}-S_w relationship prediction for the natural soils used in this work compared to that derived from the measured SWRCs. However, as with all PTFs, including the Rosetta model, it is important to understand the operational limitations of these models to ensure representative prediction of hydraulic properties.

CRediT authorship contribution statement

Jeff A.K. Silva: Conceptualization, Methodology, Validation, Formal analysis, Investigation, Resources, Writing – original draft, Writing – review & editing, Visualization, Supervision, Project administration, Funding acquisition. **Jiří Šimůnek:** Methodology, Software, Resources, Writing – review & editing. **John E. McCray:** Methodology, Writing – review & editing.

Declaration of Competing Interest

The authors declare that they have no known competing financial interests or personal relationships that could have appeared to influence

the work reported in this paper.

Acknowledgements

This material is based on work supoored by the U.S. Army Corps of Engineers and The Department of Defense Strategic Environmental Research and Development Program (SERDP) under Contract No. W912HQ18C0076.

References

Anderson, R.H., Long, G.C., Porter, R.C., Anderson, J.K., 2006. Occurrence of select perfluoroalkyl substances at U.S. Air force aqueous film-forming foam release sites other than fire252 training areas: field-validation of critical fate and transport properties. Chemosphere 150, 678–685. https://doi.org/10.1016/j.chemosphere.2016.01.014.

Anderson, R.H., Adamson, D.T., Stroo, H.F., 2019. Partitioning of poly- and perfluoroalkyl substances from soil to groundwater within aqueous film-forming foam source zones. J. Contam. Hydrol. 220, 59–65. https://doi.org/10.1016/j.jconhyd.2018.11.011.

Araujo, J.B., Brusseau, M.L., 2020. Assessing XMT-measurement variability of air-water interfacial areas in natural porous media. Water Resour. Res. 56, e2019WR025470 https://doi.org/10.1029/2019WR025470.

Araujo, J.B., Mainhagu, J., Brusseau, M.L., 2015. Measuring air–water interfacial area for soils using the mass balance surfactant-tracer method. Chemosphere 134, 199–202.

Arthur, E., Tuller, M., Moldrup, P., Resurreccion, A.C., Meding, M.S., Kawamoto, K., Komatsu, T., de Jonge, L.W., 2012. Soil specific surface area and non-singularity of soil-water retention at low saturations. Soil. Sci. Am. J. 77, 43–53.

Avnir, D., Farin, D., Pfeifer, P., 1985. Surface geometric irregularity of particulate materials: the fractal approach. J. Colloid Interface Sci. 103 (1), 112–123.

Benson, C.H., Chiang, I., Chalermyanont, T., Sawangsuriya, A., 2014. Estimating van Genuchten parameters α and n for clean sands from particle size distribution data. In: Geotechnical Special Publication No. 233, From Soil Behavior Fundamental to Innovations in Geotechnical Engineering. American Society of Civil Engineers.

Bradford, S.A., Leij, F.J., 1997. Estimating interfacial areas for multi-fluid soil systems. J. Contam. Hydrol. 27, 83–106.

Bradford, S.A., Wang, Y., Torkzaban, S., Šimůnek, J., 2015. Modeling the release of E. coli D21g with transients in water content. Water Resour. Res. 51, 3303–3316.

Brusseau, M.L., 2018. Assessing the potential contributions of additional retention processes to PFAS retardation in the subsurface. Sci. Total Environ. 613-614, 176–185.

Brusseau, M.L., 2020. Simulating PFAS transport influenced by rate-limited multi-process retention. Water Res. 168, 115179.

Brusseau, M.L., Peng, S., Schnaar, G., Costanza-Robinson, M.S., 2006. Relationships among air-water interfacial area, capillary pressure, and water saturation for a sandy porous medium. Water Resour. Res. 42, W03501.

Brusseau, M.L., Peng, S., Schnaar, G., Murao, A., 2007. Measuring air-water interfacial areas with x-ray microtomography and interfacial partitioning tracer tests. Environ. Sci. Technol. 41 (6), 1956–1961.

Brusseau, M.L., El Ouni, A., Araujo, J.B., Zhong, H., 2015. Novel methods for measuring air–water interfacial area in unsaturated porous media. Chemosphere 127, 208–213.

Brusseau, M.L., Yan, N., Van Glubt, S., Wang, Y., Chen, W., Lyu, Y., et al., 2019. Comprehensive retention model for PFAS transport in subsurface systems. Water Res. 148, 41–50.

Brusseau, M.L., Lyu, Y., Guo, B., 2020. Low-concentration tracer tests to measure air-water interfacial area in porous media. Chemosphere 250, 126305.

Chen, L., Kibbey, T.C.G., 2006. Measurement of air-water interfacial area for multiple hysteretic drainage curves in an unsaturated fine sand. Langmuir 22 (16), 6874–6880. https://doi.org/10.1021/la053521e.

Costanza-Robinson, M.S., 2001. Elucidation of Retention Processes Governing the Transport of Volatile Organic Compounds in Unsaturated Soil Systems. Ph.D. Dissertation. University of Arizona.

Costanza-Robinson, M.S., Henry, E.J., 2017. Surfactant-induced flow compromises determination of air-water interfacial areas by surfactant miscible-displacement. Chemosphere 171, 275–283.

Costanza-Robinson, M.S., Harrold, K.H., Lieb-Lappen, R.M., 2008. X-ray microtomography determination of air-water interfacial area-water saturation relationships in sandy porous media. Environ. Sci. Technol. 42 (8), 2949–2956.

Costanza-Robinson, M.S., Estabrook, B.D., Fouhey, D.F., 2011. Representative elementary volume estimation for porosity, moisture saturation, and air-water interfacial areas in unsaturated porous media: data quality implications. Water Resour. Res. 47, W07513. https://doi.org/10.1029/2010WR009655.

Dalla, E., Hilpert, M., Miller, C.T., 2002. Computation of the interfacial area for two-fluid porous medium systems. J. Contam. Hydrol. 56 (1–2), 25–48.

Dosskey, M.G., Helmers, M.J., Eisenhauer, D.E., 2006. An approach for using soil surveys to guide the placement of water quality buffers. J. Soil Water Conserv. 61 (6), 334–354.

Dullien, F.A., Zarcone, C., MacDonald, I.F., Collins, A., Bochard, R.D.E., 1989. The effects of surface roughness on the capillary pressure curves and the heights of capillary rise in glass bead packs. J. Colloid Interface Sci. 127 (2), 362–372.

El Ouni, A., Guo, B., Zhone, H., Brusseau, M.L., 2021. Testing the validity of the miscible-displacement interfacial tracer method for measuring air-water interfacial area: independent benchmarking and mathematical modeling. Chemosphere 263, 128193.

Ghanbarian, B., Hunt, A.G., Bittelli, M., Tuller, M., Arthur, E., 2021. Estimating specific surface area: Incorporating the effect of surface roughness and probing molecule size. Soil. Sci. Am. J. https://doi.org/10.1002/saj2.20231. Advance online publication.

Grant, G.P., Gerhard, J.I., 2007. Simulating the dissolution of a complex dense nonaqueous phase liquid source zone: 1. Model to predict interfacial area. Water Resour. Res. 43, W12410. https://doi.org/10.1029/2007WR006038.

Guelfo, J.L., Higgins, C.P., 2013. Subsurface transport potential of perfluoroalkyl acids at aqueous film-forming foam (AFFF)-impacted sites. Environ. Sci. Technol. 47, 4164–4171.

Guo, B., Zeng, J., Brusseau, M.L., 2020. A mathematical model for the release, transport, and retention of per- and polyfluoroalkyl substances (PFAS) in the vadose zone. Water Resour. Res. 56 (2), e2019WR026667 https://doi.org/10.1029/2019WR026667.

Gvirtzman, H., Roberts, P.V., 1991. Pore scale spatial analysis of two immiscible fluids in porous media. Water Resour. Res. 27 (6), 1165–1176.

Hamamoto, S., Moldrup, P., Kawamoto, K., Sakaki, T., Nishimura, T., Komatsu, T., 2016. Pore network structure linked by X-ray CT to particle characteristics and transport parameters. Soils Found. 56 (4), 676–690.

Jiang, H., Guo, B., Brusseau, M.L., 2019. Pore-scale modeling of fluid-fluid interfacial area in variably saturated porous media containing microscale surface roughness. Water Resour. Res. 56, e2019WR025876 https://doi.org/10.1029/2019WR025876.

Kakare, M.V., Fort, T., 1996. Determination of the air-water interfacial area in wet "unsaturated" porous media. Langmuir 12 (8), 2041–2044.

Kibbey, T.C.G., 2013. The configuration of water on rough natural surfaces: implications for understanding air-water interfacial area, film thickness, and imaging resolution. Water Resour. Res. 49, 4765–4774. https://doi.org/10.1002/wrcr.20383.

Kibbey, T.C.G., Chen, L., 2012. A pore network model study of the fluid-fluid interfacial areas measured by dynamic-interface tracer depletion and miscible displacement water phase advective tracer methods. Water Resour. Res. 48, W10519. https://doi.org/10.1029/2012WR011862.

Kim, H., Rao, P.S.C., Annable, M.D., 1997. Determination of effective air-water interfacial area in partially saturated porous media using surfactant adsorption. Water Resour. Res. 33 (12), 2705–2711.

Kim, H., Rao, P.S.C., Annable, M.D., 1999. Gaseous tracer technique for estimating air-water interfacial areas and interface mobility. Soil Soc. Am. J. 63, 1554–1560.

Leverett, M.C., 1941. Capillary behavior in porous solids. Trans. Am. Inst. Min. Merall. Pet. Eng. 142, 152–169.

McDonald, K., Carroll, K.C., Brusseau, M.L., 2016. Comparison of fluid-fluid interfacial areas measured with x-ray microtomography and interfacial partitioning tracer tests for the same samples. Water Resour. Res. 52 (7), 5393–5399. https://doi.org/10.1002/2016WR018775.

McKenzie, E.R., Siegrist, R.L., McCray, J.E., Higgins, C.P., 2016. The influence of a nonaqueous phase liquid (NAPL) and chemical oxidant application of perfluoroalkyl acid (PFAA) fate and transport. Water Res. 92, 199–207.

Oostrom, M., White, M.D., Brusseau, M.L., 2001. Theoretical estimation of free and entrapped non-wetting fluid interfacial areas in porous media. Adv. Water Resour. 24, 887–898.

Or, D., Tuller, M., 1999. Liquid retention and interfacial area in variably saturated porous media: upscaling from single-pore to sample-scale model. Water Resour. Res. 35 (12), 3591–3605.

Peng, S., Brusseau, M.L., 2005. Impact of soil texture on air-water interfacial areas in unsaturated sandy porous media. Water Resour. Res. 41, W03021. https://doi.org/10.1029/2004WR003233.

Peng, S., Brusseau, M.L., 2012. Air-water interfacial area and capillary pressure: porous-medium texture effects and an empirical function. J. Hydrol. Eng. 17 (7) https://doi.org/10.1061/(ASCE)HE.1943-5584.0000515.

Pfeifer, P., Avnir, D., Farin, D., 1983. Ideally irregular surfaces, of dimension greater than two, in theory and practice. Surf. Sci. 126, 569–572. https://doi.org/10.1016/0039-6028(83)90759-8.

Sakaki, T., Illangasekare, T.H., 2007. Comparison of height-averaged and point-measured capillary pressure-saturation relations for sands using a modified Tempe cell. Water Resour. Res. 43, W12502. https://doi.org/10.1029/2006WR005814.

Schaap, M.G., Leij, F.J., van Genuchten, M.Th., 2001. Rosetta: a computer program for estimating soil hydraulic parameters with hierarchical pedotransfer functions. J. Hydrol. 251, 163–176.

Schaefer, C.E., DiCarlo, D.A., Blunt, M.J., 2000. Experimental measurement of air-water interfacial area during gravity drainage and secondary imbibition in porous media. Water Resour. Res. 36 (4), 885–890.

Schroth, M.H., Ahearn, S.J., Selker, J.S., Istok, J.D., 1996. Characterization of Miller-similar silica sands for laboratory hydrologic studies. Soil Sci. Soc. Am. J. 60, 1331–1339.

Schroth, M.H., Oostrom, M., Dobson, R., Zeyer, J., 2008. Thermodynamic model for fluid-fluid interfacial areas in porous media for arbitrary drainage-imbibition sequences. Vadose Zone J. 7, 966–971. https://doi.org/10.2136/vzj2007.0185.

Shin, H.-M., Viery, V.M., Ryan, P.B., Detwiler, R., Sanders, B., Steenland, K., Bartell, S. M., 2011. Environmental fate and transport modeling for perfluorooctanoic acid emitted from the Washington works Facility in West Virginia. Environ. Sci. Technol. 45 (4), 1435–1442.

Silva, J.A.K., 1997. Retention Processes Affecting VOC Vapor Transport in Water-Unsaturated Porous Media. MSc Thesis. University of Arizona, Tucson, AZ.

Silva, J.A.K., Bruant, R.G., Conklin, M.H., Corley, T.L., 2002. Equilibrium partitioning of chlorinated solvents in the vadose zone: low foc geomedia. Environ. Sci. Technol. 36 (7), 1613–1619.

Silva, J.A.K., Martin, W.A., Johnson, J., McCray, J.E., 2019. Evaluating air-water and NAPL-water interfacial adsorption and retention of Perfluorocarboxylic acids within the vadose zone. J. Contam. Hydrol. 223, 103472.

Silva, J.A.K., Šimůnek, J., McCray, J.E., 2020. A modified HYDRUS model for simulating PFAS transport in the vadose zone. Water 12, 2758. https://doi.org/10.3390/w12102758.

Šimůnek, J., van Genuchten, M.Th., Šejna, M., 2016. Recent developments and applications of the HYDRUS computer software packages. Vadose Zone J. 15 (7), 25. https://doi.org/10.2136/vzj2016.04.0033.

Sweijen, T., Aslannejad, H., Hassanizadeh, M., 2017. Capillary pressure-saturation relationships for porous granular materials: pore morphology method vs. pore unit assembly method. Adv. Water Resour. 107, 22–31.

Torrens, J.L., Herman, D.C., Miller-Maier, R., 1998. Biosurfactant (Rhamnolipid) sorption and the impact on Rhamnolipid-facilitated removal of cadmium from various soils under saturated flow conditions. Environ. Sci. Technol. 32 (6), 776–781.

van Genuchten, M.Th., 1980. A closed-form equation for predicting the hydraulic conductivity of unsaturated soils. Soil Sci. Soc. Am. J. 44, 892–898.

van Glubt, S., Brusseau, M.L., Ni, Y., Huang, D., Khan, N., Carroll, K.C., 2021. Column versus batch methods for measuring PFOS and PFOA sorption to geomedia. Environ. Pollut. 268, 115917.

Wang, K., Zhang, R., Wang, F., 2005. Testing of pore-solid fractal model for the soil water retention function. Soil Sci. Soc. Am. J. 69, 776. https://doi.org/10.2136/sssaj2004.0247.

Wang, J.-P., Lambert, P., De Kock, T., Cnudde, V., Francois, B., 2019. Investigation of the effect of specific interfacial area on strength of unsaturated granular materials by x-ray tomography. Acta Geotech. 14, 1545–1559.

Weber, A.K., Barber, L.B., LeBlanc, D.R., Sunderland, E.M., Vecitis, C.D., 2017. Geochemical and hydrologic factors controlling subsurface transport of poly- and perfluoroalkyl substances, Cape Cod, Massachusetts. Environ. Sci. Technol. 51, 4269–4279.

Wenzel, R.N., 1936. Resistance of solid surfaces to wetting by water. J. Ind. Eng. Chem. 28 (8), 988–994.

Xiao, F., Simcik, M.F., Halbach, T.R., Gulliver, J.S., 2015. Perfluorooctane sulfonate (PFOS) and perfluorooctanoate (PFOA) in soils and groundwater of a US metropolitan area: migration and implications for human exposure. Water Res. 72, 64–74.

Yang, H., Rahardjo, H., Leong, E., Fredlund, D., 1994. Factors affecting drying and wetting soil-water characteristic curves of sandy soils. Can. Geotech. J. 41, 908–920.

Yang, H., Baudet, B.A., Ya, T., 2016. Characterization of the surface roughness of sand particles using an advanced fractal approach. Proc. R. Soc. A 472, 20160524.

Zheng, W., Yu, X., Jin, Y., 2015. Considering surface roughness effects in a triangular pore space model for unsaturated hydraulic conductivity. Vadose Zone J. 14 (7) https://doi.org/10.2136/vzj2014.09.0121 vzj2014.09.0121.